J Mol Model (2016) 22: 237
DOI 10.1007/s00894-016-3107-9

ORIGINAL PAPER

Theoretical study on the metabolic mechanisms of levmepromazine by cytochrome P450

Yongting Wang[1] · Qiu Chen[1] · Zhiyu Xue[1] · Yan Zhang[1] · Zeqin Chen[1] · Ying Xue[2]

Received: 4 July 2016 / Accepted: 1 September 2016 / Published online: 13 September 2016

Abstract Levomepromazine, an "older" typical neuroleptic, is widely applied in psychiatry for the treatment of schizophrenia. The biotransformation of Levomepromazine remains elusive up to now, but found to result in the formation of different derivatives that may contribute to the therapeutic and/or side-effects of the parent drug. The present work aims to resolve the metabolic details of Levomepromazine catalyzed by cytochrome P450, an important heme-containing enzyme superfamily, based on DFT calculation. Two main metabolic pathways have been addressed, S-oxidation and N-demethylation. The mechanistic conclusions have revealed a stepwise transfer of two electrons mechanism in S-oxidation reaction. N-demethylation is a two-step reaction, including the rate-determining N-methyl hydroxylation which proceeds via the single electron transfer (SET) mechanism and the subsequent C-N bond fission through a water-assisted enzymatic proton-transfer process. N-demethylation is more feasible than S-oxidation due to its lower activation energy and N-desmethyllevomepromazine therefore is the most plausible metabolite of Levomepromazine. Each metabolic pathway proceeds in a spin-selective manner (SSM) mechanism, predominately via the LS state of Cpd I. Our observations are in good accordance with the experimental results, which can provide some general implications for the metabolic mechanism of Levomepromazine-like drugs.

Keywords Levomepromazine · Cytochrome P450 · Metabolic mechanism · N-demethylation · S-oxidation

Yongting Wang and Qiu Chen contributed equally to this work.

Electronic supplementary material The online version of this article (doi:10.1007/s00894-016-3107-9) contains supplementary material, which is available to authorized users.

✉ Zeqin Chen
chenzeqin@cwnu.edu.cn

[1] College of Chemistry and Chemical Engineering, Chemical Synthesis and Pollution Control Key Laboratory of Sichuan Province, China West Normal University, Nanchong 637002, People's Republic of China

[2] College of Chemistry, Key Laboratory of Green Chemistry and Technology in Ministry of Education, Sichuan University, Chengdu 610064, People's Republic of China

Introduction

Levomepromazine (LM), known as methotrimeprazine, belongs to the group of phenothiazine neuroleptics with an aliphatic side-chain. It is an "older" typical neuroleptic with low antipsychotic potency first used in psychiatry for the treatment of schizophrenia [1]. Although lots of new atypical neuroleptic drugs have emerged for psycho-pharmacotherapy up to now, LM is still widely applied in the therapy of different psychiatric and non-psychiatric states [2, 3] as well as in the control of symptoms in palliative care as an antipsychotic, anxiolytic, antimimetic, and sedative drug [4]. The antipsychotic effect of LM is mainly due to its action as a moderate antagonist of the dopaminergic D2 receptor. Besides, LM also acts as an antagonist of the adrenergic a1 and the muscarinic M1 receptors, which is associated with some side-effects of the drug, such as, sedation, hypotension, and anticholinergic symptoms [5, 6]. Compared to haloperidol, LM causes fewer extrapyramidal side-effects [7].

Like other phenothiazine derivatives, LM is extensively metabolized in the body before being excreted. Two metabolic routes, S-oxidation and N-demethylation, were reported to be the dominant biotransformation pathways of LM in humans (Scheme 1) [8–10]. N-desmethyllevomepromazine, the N-demethylated metabolite, showed an almost equally potent

Scheme 1 The main metabolic pathways of LM catalyzed by cytochrome P450

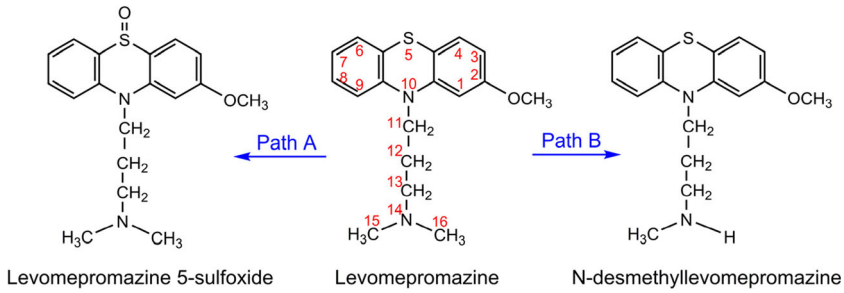

receptor binding activity (dopaminergic and a1- adrenergic) as did the parent drug, whereas the 5-sulfoxide was considerably less active in this respect [6, 11, 12]. Thus, the biotransformation of LM leads to the formation of different derivatives that display biological activity and may contribute to the therapeutic and/or side-effects of the parent drug.

Cytochrome P450, an important heme-containing enzyme superfamily, is potentially responsible for the metabolism of LM. The experimental work performed in vitro using cDNA-expressed human CYP isoforms has indicated that CYP3A4 is the main isoform responsible for S-oxidation (72 %) and N-demethylation (78 %) at a therapeutic concentration of LM (10 mM), while CYP1A2 contributes to a lesser degree to S-oxidation (20 %) [13]. It can be negligible (0.1–8 %) for CYP2A6, CYP2B6, CYP2C8, CYP2C9, CYP2C19, CYP2D6, and CYP2E1 in catalyzing the above-mentioned reactions. At a higher and toxicological concentration of the neuroleptic (100 mM), however, the role of CYP1A2 to LM metabolism obviously increases (from 20 to 28 % for 5-sufoxidation, and from 8 to 32 % for N-demethylation), whereas the relative contribution of CYP3A4 dramatically decreases (from 72 to 59 % for S-oxidation, and from 78 to 47 % for N-demethylation).

In spite of the wide and long-time use of LM, the mechanic details of LM metabolism by cytochrome P450 is still unclear so far. The aim of the present study was to discover the metabolic mechanisms of LM by cytochrome P450 using the density functional theoretic (DFT) calculations. This observation can provide some essential clues for the further psychopharmacotherapy study.

Methods

All DFT calculations were performed using the Gaussian 09 suite of programs [14]. The active species of cytochrome P450 in catalysis is believed to be a Fe^{IV}=O complex with a porphyrin radical, referred to as compound I (Cpd I in brief) [15]. A popular six-coordinate oxo-ferryl species model, $Fe^{4+}O^{2-}(C_{20}N_4H_{12})^{-}(SH)^{-}$ [16], was employed as the reactive Cpd I, which contains a truncated heme and a thiolate axial ligand (SH-) built from the crystal structure of CYP3A4 (PDB ID: 1TQN) [17]. The spin-unrestricted hybrid functional UB3LYP was adopted for the optimization of all the stationary points without symmetry constraints at the LACVP(Fe)/6-31G (H, C, N, O, S) basis set (B1 in brief). These model and computational methods chosen have been tested extensively and proven to be reliable in solving cytochrome P450 enzymes problems [18–24]. Transition states were affirmed by harmonic frequency analysis to possess only one imaginary frequency and the stationary points were confirmed as minima with all positive frequencies. The validity of the TS geometry was verified by intrinsic reaction coordinate (IRC) calculations [25]. Natural population atomic (NPA) charges were determined using Reed and Weinhold's natural bond orbital (NBO) analysis [26].

To obtain more reliable energetics, single-point calculations were performed using UB3LYP and dispersion corrected spin-unrestricted hybrid functional of UB3LYP-D3 with two higher basis sets, 6-311+G* and 6-311++G** (B2 and B3 in brief). The calculated energetics is collected in Table S1 of the Supporting information (SI) document for comparison. It can be seen from Table S1 that the dispersion-corrected activation energies are lower than those without dispersion correction by 2–5 kcal mol^{-1}. So dispersion correction should be included in the calculation. Furthermore, the activation energies calculated at B2 basis set are close to those at B3 basis set with the deviation of no more than 2.2 kcal mol^{-1}. No matter what basis set is considered, the DFT calculations consistently predict the reactivity patterns and the conclusions drawn here. And therefore, our following discussions focus on the energetics obtained by UB3LYP-D3 functional with the B2 basis set. All of the single-point energies were corrected by the gas-phase thermodynamic quantities. The thermodynamic data reported in this paper are at 298.15 K and 1 atm.

Results and discussion

In the present work, two main metabolic pathways (Scheme 1) were characterized for LM by cytochrome P450, including oxidation at the S_5 site of the thiazine ring (S-oxidation, path A) and N-demethylation at N_{14} site (path B). A nomenclature was adopted to characterize each stationary point for clear illustration. Reactant complex, transition state, intermediate, and product complex were abbreviated as RC, TS, IM, and PC,

respectively. Considering the high-spin (HS) quartet and low-spin (LS) doublet states of the active species Cpd I, a number at the top left corner denotes the multiplicity, "2" for the LS state and "4" for the HS state. Another number at the bottom right corner denotes the reaction step: "1" standing for the first step and "2" for the second step. For example, A-^{2}RC and A-^{4}RC represent the LS and HS reactant complexes along path A, while B-^{2}TS$_1$ and B-^{4}TS$_1$ represents the LS and HS transition states involved in the first step of path B. The complete depiction of the metabolic mechanisms is presented in Scheme 2. Each pathway is discussed in detail below.

S-oxidation (path A)

As depicted in Scheme 2a, S-oxidation is a one-step reaction, which involves the direct oxidation of S_5 atom by Cpd I. The optimized geometries of all the stationary points are presented in Fig. 1. The located transition state A-TS$_1$ species, A-^{2}TS$_1$ and A-^{4}TS$_1$, is characterized by its single imaginary frequency of 151.2i cm^{-1} LS and 610.8i cm^{-1} HS. It implies that heavy oxygen atom motion is comprised in the reaction vector. Animation of the single imaginary frequency of A-TS$_1$ species indicates the motion of oxygen atom from Fe to S_5 atom, leading to Fe-O_5 bond breakage and S_5-O bond formation. The Fe-O_5 bond in transition state A-TS$_1$ species is elongated by 0.056 Å LS and 0.169 Å HS with respect to their corresponding reactant complex A-RC species, A-^{2}RC and A-^{4}RC. This is concomitant with the remarkable curtailment of the S_5–O distance with 2.322 Å LS and 2.055 Å HS. It can be readily seen that, in A-TS$_1$ species, the oxygen atom is closer to the iron atom ($r_{Fe\text{-}O}$=1.708 Å LS and 1.823 Å HS) than to the sulfur atom. A-TS$_1$ species therefore is more reactant-like in character. More especially, this reactant-like character of A-^{2}TS$_1$ is more striking than A-^{4}TS$_1$. In the product complex A-PC species, A-^{2}PC and A-^{4}PC, a double bond is formed between sulfur S_5 and oxygen atoms ($r_{S\text{-}O}$=1.731 Å LS and 1.703 Å HS). Concomitantly, the Fe–O bond is elongated to be 2.022 Å LS and 2.348 Å HS.

The LS and HS energy profiles for S–oxidation are presented in Fig. 2. As shown in Fig. 2a, the gas-phase LS/HS activation energy is 4.3/9.8 kcal mol^{-1} at the UB3LYP/B2//B1 level. This oxidation process is exothermic with the reaction energy of 27.8 kcal mol^{-1} LS and 22.0 kcal mol^{-1} HS. The lower LS energy barrier is in good accordance with the more striking reactant-like character of A-^{2}TS$_1$ than A-^{4}TS$_1$. Originating from the HS and LS states of Cpd I, theoretical studies have revealed two possible mechanisms: the spin-selective manner (SSM) scenario and the two-state reactivity (TSR) [27]. The energy gap between A-^{2}TS$_1$ and A-^{4}TS$_1$ in the present work is large at 5.5 kcal mol^{-1}. The ratio of the reaction rate on the LS:HS route is 1.1×10^4:1. As a consequence, S-oxidation of LM by Cpd I proceeds mainly in an SSM mechanism. The LS state of Cpd I is thermodynamically and kinetically more favorable than HS state.

The spin density distribution for the stationary points involved in S-oxidation is shown in Table 1. In the A-RC species, spin density mainly resides on Cpd I. As the reaction begins, it transfers gradually from the oxygen, −SH ligand, and porphyrine to the iron and sulfur atom of LM. In A-TS$_1$ species, the accumulation of spin density on sulfur atom indicates the partial formation of S-O and

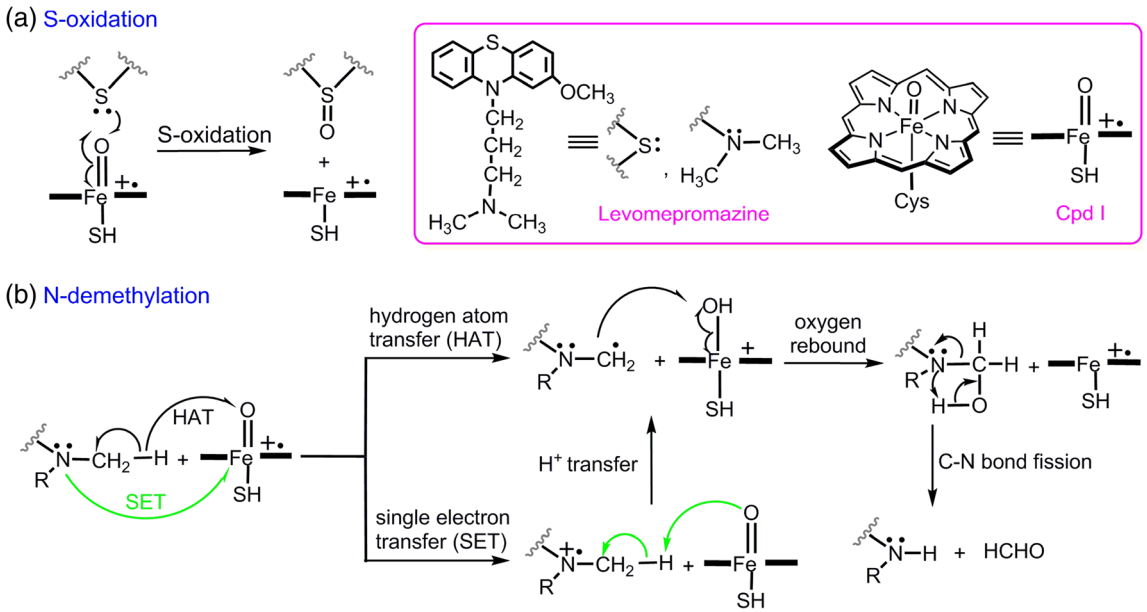

Scheme 2 Metabolic mechnisms of LM catalyzed by cytochrome P450 enzyme

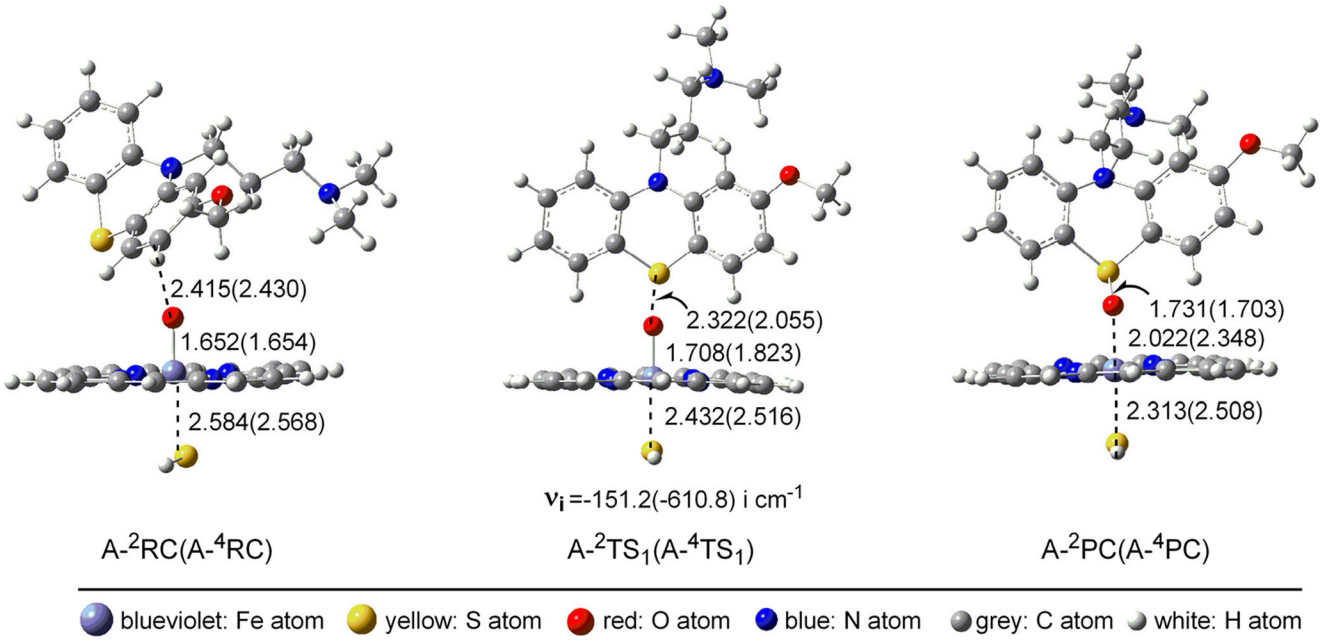

Fig. 1 Optimized structures (in Å) for S–oxidation (path A) of LM by Cpd I at the UB3LYP/B1 level (values out of parentheses, geometrical parameters on the LS state; values in parentheses, geometrical parameters on the HS state. ν_i represents for the single imaginary frequency of the transition state. Atom and symbol definitions are the same in Figs. 3, 4, and 5)

Fe-O single bonds, leading to the occurrence of an unpaired electron on the sulfur atom. As the reaction proceeds, the unpaired electron on sulfur further pairs with the electron of the oxygen atom residing on Fe-O single bond to produce the S=O double bond in A-PC species. Simultaneously, Fe-O single bond is cleaved. There is no spin density on sulfur atom any more. Spin density is mainly localized on iron both on the LS and the HS states in A-PC species. All the above results clearly show a stepwise transfer of two electrons.

N-demethylation (path B)

As depicted in Scheme 2b, the overall reaction of N-demethylation of LM is stepwise, including the initial N-methyl hydroxylation and subsequent C-N bond fission. For N-methyl hydroxylation, the reaction model begins with proton transfer from the methyl group to the Cpd I's oxygen atom, forming a N-methylene intermediate, which then acts as a receptor of hydroxyl from the active iron species through a oxygen-rebound process. The reaction is concerted both on

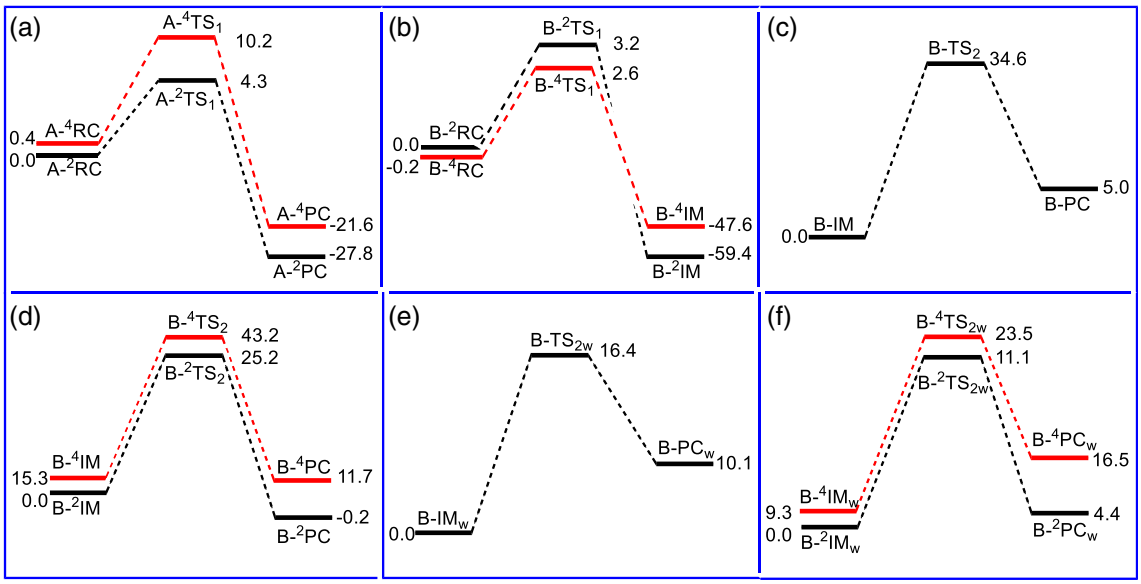

Fig. 2 Energy profiles (in kcal mol^{-1}) for S-oxidation (**a**) and N–demethylation (**b-f**) of LM by Cpd I at the UB3LYP/B2//B1 level

Table 1 Spin densities for the species in the S-oxidation of LM by Cpd I at the UB3LYP/B1 level

	Cpd I				LM	
	Fe	O	SH	Por[a]	S	Other
A-^{2}RC	1.22	0.88	−0.58	−0.52	0.00	0.00
A-^{2}TS$_1$	1.40	0.35	−0.22	−0.24	−0.24	−0.05
A-^{2}PC	1.07	0.01	0.01	−0.09	0.00	0.00
A-^{4}RC	1.09	0.93	0.53	0.44	0.00	0.00
A-^{4}TS$_1$	2.00	0.37	0.43	−0.03	0.19	0.04
A-^{4}PC	2.69	0.06	−0.15	0.40	0.00	0.01

[a] Por = porphyrine

the LS and HS states, forming a carbinolamine-heme complex without a distinct oxygen-rebound step.

N-methyl hydroxylation The optimized geometries of all the stationary points for the N-methyl hydroxylation of path B are shown in Fig. 3. The located transition state B-TS$_1$ species, B-^{2}TS$_1$ and B-^{4}TS$_1$, is characterized by its single imaginary frequency of 575.2i cm^{-1} LS and 1023.9i cm^{-1} HS. Animation of the single imaginary frequency of B-TS$_1$ species shows the motion of hydrogen from methyl carbon atom to the oxygen atom of Cpd I atom. Obviously, the Fe-O bond is elongated by 0.047 Å LS and 0.082 Å HS in the transition state B-TS$_1$ species with respect to the reactant complex B-RC species, B-^{2}RC and B-^{4}RC, whereas the O-H distance is considerably reduced by 0.782 Å LS and 0.902 HS. This is concurrent with the elongation of the C–H bond by 0.079 Å LS and 0.175 Å HS. Transition state B-TS$_1$ species is characterized by an almost collinear arrangement of the C-H-O atoms with the bond angles of 172.2° LS and 171.7° HS. The above geometric parameters show the different degree of C-H bond breakage in the B-TS$_1$ species. The transferred hydrogen atom is closer to the carbon atom ($r_{C\text{-}H}$=1.183 Å LS and 1.280 Å HS) than to the oxygen atom ($r_{O\text{-}H}$=1.483 Å LS and 1.301 Å HS). Therefore, B-TS$_1$ species is still more reactant-like in character. As the reaction progresses from B-RC species to the intermediate B-IM species, B-^{2}IM$_1$ and B-^{4}IM$_1$, the distances between the SH ligand and Fe is shortened by 0.283 Å LS and 0.058 Å HS. The Fe–O bond is elongated to be 2.083 Å LS and 2.500 Å HS in B-IM species.

The calculated energy profiles for the N-methyl hydroxylation of path B are shown in Fig. 2b. The gas-phase LS/HS activation energy is 3.2/2.8 kcal mol^{-1} for B-TS$_1$ species at the UB3LYP/B2//B1 level. The energy gaps between LS and HS of B-^{2}TS$_1$ is small at 0.4 kcal mol^{-1}. The ratio of the reaction rate on the LS:HS route is 1.9:1, indicating that the N-methyl hydroxylation proceeds in a TSR mechanism. The N-methyl hydroxylation is greatly exothermic with the reaction energy of 59.4 kcal mol^{-1} LS and 47.4 kcal mol^{-1} HS.

As for the N-methyl hydroxylation step, two controversial mechanisms, single electron transfer (SET) [28, 29] versus hydrogen atom transfer (HAT) [30, 31], have existed for decades in the literature (Scheme 2). There are not any standard rules to generalize their application, since the preferred mechanism is dependent on the detailed characteristics of the amine [32]. The spin density distribution for the stationary points involved in the N-methyl hydroxylation of path B is reported in Table 2. Initially, spin density is also mainly localized on Cpd I. Then, with the transfer of the hydrogen atom, it shifts from oxygen, −SH ligand, and porphyrine to the iron and nitrogen atom of LM. In B-TS$_1$ species, high spin density resides mainly on the nitrogen atom of LM and the iron and there is some spin density on the carbon atom in B-^{4}TS$_1$, which contributes to the stabilization of carbon during the leaving of the hydrogen atom. In B-^{4}TS$_1$, excess unpaired spin is no longer observed on the porphyrine and spin density is delocalized between Fe-oxo and –SH. In the B-IM species, spin density mainly resides on iron both on the LS and HS

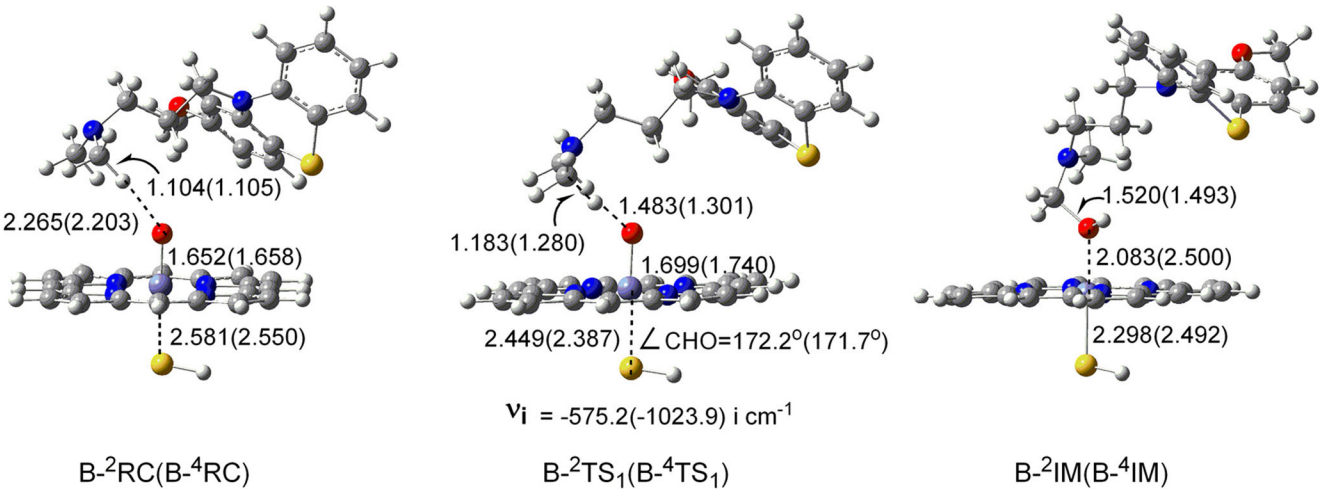

Fig. 3 Optimized structures (in Å) for the N-methyl hydroxylation in N–demethylation (path B) of LM by Cpd I at the UB3LYP/B1 level

Table 2 Spin densities for the species in the N-methyl hydroxylation of LM by Cpd I at the UB3LYP/B1 level

	Cpd I				LM			
	Fe	O	SH	Por	H	C	N	rest
B-^{2}RC	1.21	0.88	−0.55	−0.50	0.00	0.00	−0.04	0.00
B-^{2}TS$_1$	1.57	0.38	−0.21	−0.26	−0.03	−0.07	−0.33	−0.04
B-^{2}IM$_1$	1.08	0.00	0.00	−0.09	0.00	0.00	0.00	0.00
B-^{4}RC	1.07	0.95	0.49	0.39	0.00	0.01	0.07	0.01
B-^{4}TS$_1$	1.41	0.72	0.25	−0.02	0.01	0.25	0.35	0.03
B-^{4}IM	2.90	0.01	0.11	−0.03	0.00	0.00	0.00	0.00

states. All the above observations imply that this N-methyl hydroxylation proceeds in the SET mechanism.

C-N bond fission As the second step of the N-demethylation, C-N bond fission requires a proton transfer from the hydroxyl oxygen to the nitrogen atom. Four different processes for C-N bond fission were examined, C-N bond direct fission and the water-assisted C-N bond fission under the enzymatic and non-enzymatic environments. The energy profiles and optimized structures of all the stationary point are depicted in Figs. 2, 4, and 5, respectively.

For the C-N bond direct fission process, the enzymatic and non-enzymatic transition states (B-^{2,4}TS$_2$ and B-TS$_2$) shown in Fig. 4 are all rhomboid structures formed by nitrogen, carbon, oxygen, and hydrogen atoms, whose single imaginary frequencies are greater than 1456i cm^{-1}. Animation of the single imaginary frequency shows the direct motion of the hydroxyl hydrogen to the nitrogen atom. The gas-phase enzymatic LS/HS and non-enzymatic activation energies are 25.2/27.9 and 34.6 kcal mol^{-1}, respectively, at the UB3LYP/B2//B1 level (Fig. 2c and d), indicating that the enzymatic C-N bond fission is kinetically more favorable than the non-enzymatic process. Even so, large activation energy is still involved in the

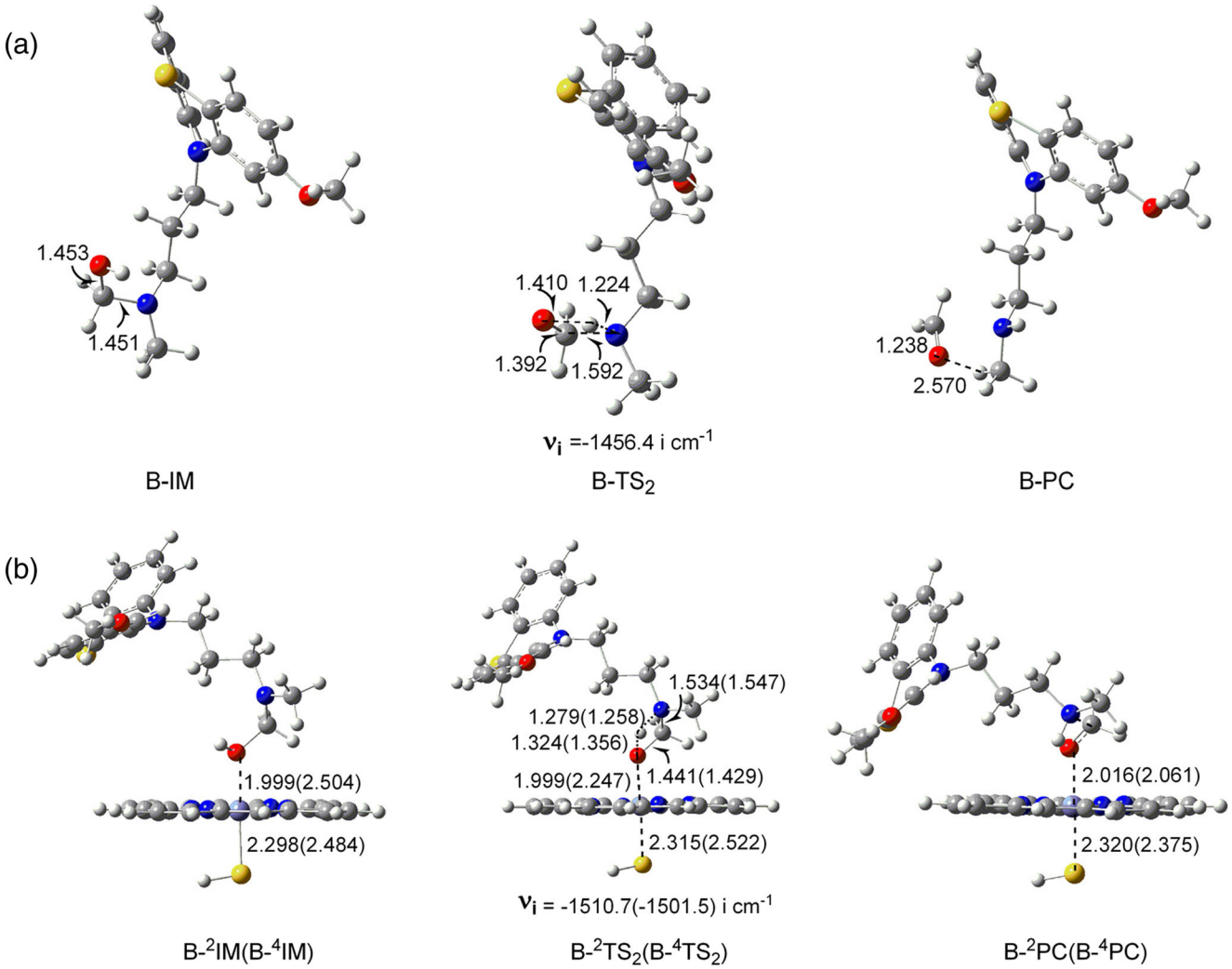

Fig. 4 Optimized structures (in Å) for the non-enzymatic (**a**) and enzymatic (**b**) C-N direct fission along the N-demethylation of LM by Cpd I at the UB3LYP/B1 level

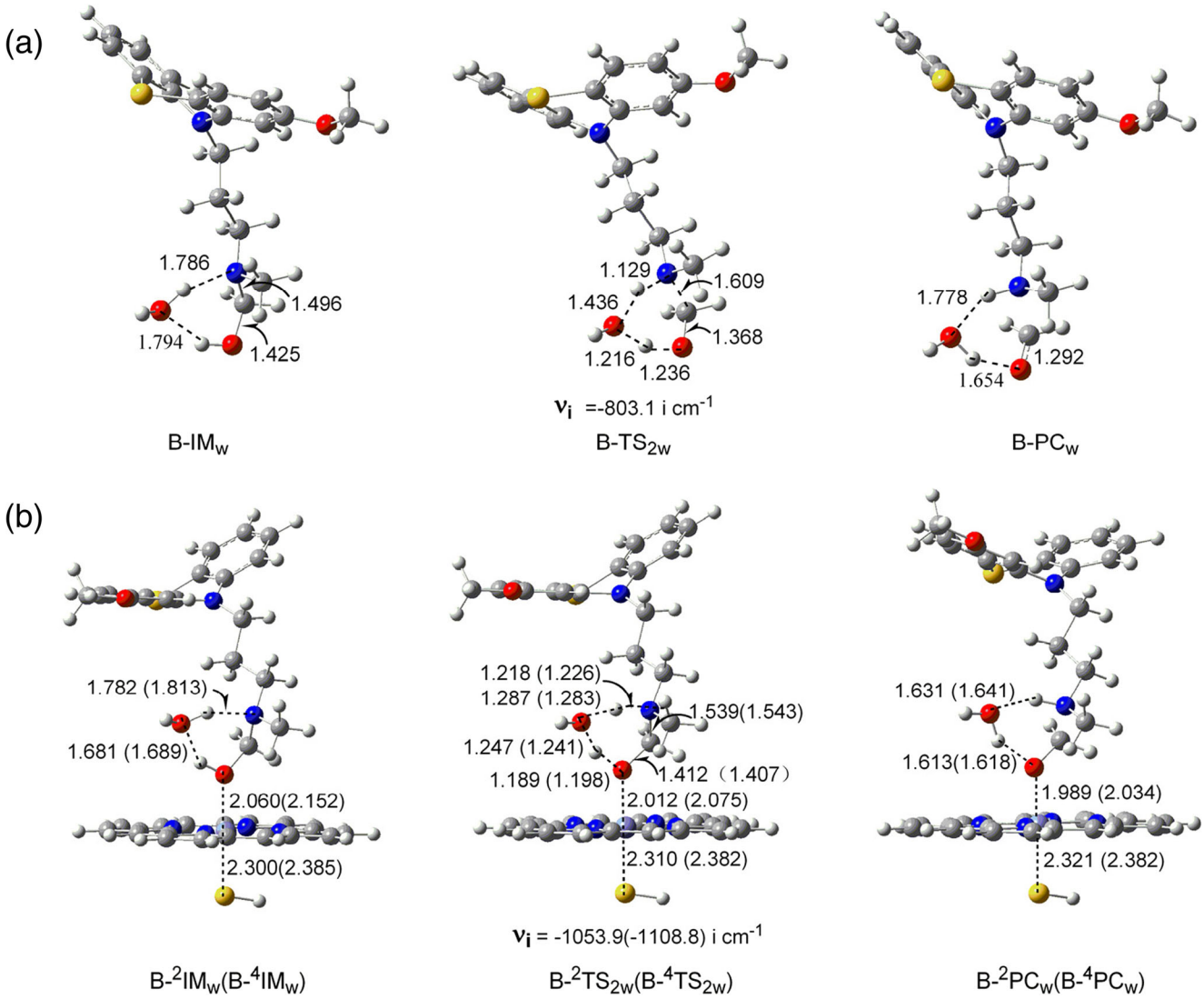

Fig. 5 Optimized structures (in Å) for the non-enzymatic (**a**) and enzymatic (**b**) water-assisted C-N fission along the N-demethylation (path B) of LM by Cpd I at the B1 level

enzymatic C-N bond direct fission process attributed to the high angle strains in the rhomboid transition state structures. Then, to relax these transition states and reduce the angle strain, one explicit water molecule was added to assist the transfer of a proton.

With the assistance of the one-water-bridge, receiving a proton and donating one in turn, the located enzymatic and non-enzymatic transition states (B-^{2,4}TS$_{2w}$ and B-TS$_{2w}$) are expanded to be hexagon structures (Fig. 5). Their single imaginary frequencies range from 803~1109i cm^{-1}, wherein the water molecule hydrogen-bonding with the nitrogen gradually transfers a proton to the nitrogen, while the hydroxyl proton gradually transfers to the water oxygen. It can be seen from Fig. 2e and f that the gas-phase enzymatic LS/HS and non-enzymatic activation energies of the water-assisted C-N bond fission processes are 11.1/14.2 and 16.4 kcal mol^{-1}, respectively, at the UB3LYP/B2//B1 level. Then, with the assistance of one explicit water molecule, the enzymatic LS/HS activation energy is 5.3/2.2 kcal mol^{-1} lower than the non-enzymatic process. Clearly, the activation energies required for the water-assisted C-N bond fission processes are obviously lower than the C-N bond direct fission processes by 13~19 kcal mol^{-1}. The large activation energy savings is derived from the smaller ring tension of the hexagon compared to rhomboid. The energy gap between B-^{2}TS$_{2w}$ and B-^{4}TS$_{2w}$ is 3.1 kcal mol^{-1}. The ratio of the reaction rate on the LS:HS route is 18.7:1. Furthermore, the energy of B-^{4}IM$_{2w}$ on the HS state is 9.3 kcal mol^{-1} larger than B-^{2}IM$_{2w}$ on the LS state. Then, the fission of C-N bond proceeds mainly in an SSM mechanism, predominately via the enzymatic water-assisted proton transfer process on the LS state. As a consequence, N-methyl hydroxylation should be the rate-determining step of path B due to its high gas-phase activation energy and large exothermic property along the potential energy surface.

In summary, the LS/HS activation barriers for the rate-determining steps of S-oxidation (path A) and N-demethylation (path B) are 4.3/9.8 and 3.2/2.8 kcal mol^{-1}, respectively. It can be concluded that N-demethylation is the most plausible metabolic pathway of LM catalyzed by cytochrome P450 either on the LS or HS state. Therefore, N-desmethyllevomepromazine (B-PC) is the optimum metabolite of LM. All the observations agree well with the experimental results [13]. All the metabolic pathways proceed predominately through the LS state of Cpd I.

Conclusions

Two main metabolic mechanisms of LM catalyzed by cytochrome P450 have been characterized in the present work based on DFT calculation, including S-oxidation (path A) and N-demethylation (path B). The mechanistic conclusions have revealed that S-oxidation involves a stepwise transfer of two electrons, while N-demethylation is a two-step reaction, comprising the rate-determining N-methyl hydroxylation and subsequent C-N bond fission which occurs predominately via a water-assisted enzymatic process. N-methyl hydroxylation proceeds via the SET mechanism. N-demethylation is thermodynamically and kinetically more favorable than S-oxidation and N-desmethyllevomepromazine therefore is the most feasible LM metabolite catalyzed by cytochrome P450. Each metabolic pathway proceeds predominately via the LS state of Cpd I. Our observations agree well with the experimental results, which can provide some general implications for the metabolic mechanism of LM-like drugs.

Acknowledgments This work was supported by grants from National Natural Science Foundation of China (Grant No. 21203153), Science & Technology Department of Sichuan Province (Grant No. 2011JY0136) and Department of Education of Sichuan Province (Grant No. 12ZA174) and China West Normal University (Grant No. 11B002).

References

1. Sivaraman P, Mitra A, Jayaram MB (2012) Levomepromazine for schizophrenia. Cochrane Database Syst Rev 38:219–220
2. Gjerden P, Slørdal L, Bramness JG (2010) Prescription persistence and safety of antipsychotic medication: a national registry-based 3-year follow-up. Eur J Pharmacol 66:911–917
3. Green B, Pettit T, Faith L, Seaton K (2004) Focus on levomepromazine. Curr Med Res Opin 20:1877–1881
4. Dietz I, Schmitz A, Lampey I, Schulz C (2013) Evidence for the use of Levomepromazine for symptom control in the palliative care setting: a systematic review. BMC Palliat Care 1:1
5. Bylund DB (1981) Interactions of neuroleptic metabolites with dopaminergic, alpha adrenergic and muscarinic cholinergic receptors. J Pharmacol Exp Ther 217:81–86
6. Hals PA, Hall H, Dahl SG (1986) Phenothiazine drug metabolites: dopamine D2 receptor, α 1-and α 2-adrenoceptor binding. Eur J Pharmacol 125:373–381
7. Lal S, Thavundayil JX, Nair NV, Annable L (2006) Levomepromazine versus chlorpromazine in treatment-resistant schizophrenia: a double-blind randomized trial. J Psychiatry Neurosci 31:271–279
8. Johnsen HELGE, Dahl SG (1982) Identification of O-demethylated and ring-hydroxylated metabolites of methotrimeprazine (levomepromazine) in man. Drug Metab Dispos 10:63–67
9. Hals PA, Dadl SG (1995) Metabolism of LM in man. Eur J Drug Metab Pharmacokinet 20:61–71
10. Jorgensen A (1986) Metabolism and pharmacokinetics of antipsychotic drugs. Prog Drug Metab 9:111–174
11. Dahl SG, Hjorth M, Hough E (1982) Chlorpromazine, methotrimeprazine, and metabolites. Structural changes accompanying the loss of neuroleptic potency by ring sulfoxidation. Mol Pharmacol 21:409–414
12. Dahl SG, Hall H (1981) Binding affinity of levomepromazine and two of its major metabolites to central dopamine and α-adrenergic receptors in the rat. Psychopharmacology 74:101–104
13. Wójcikowski J, Basińska A, Daniel WA (2014) The cytochrome P450-catalyzed metabolism of levomepromazine: a phenothiazine neuroleptic with a wide spectrum of clinical application. Biochem Pharmacol 90:188–195
14. Frisch MJ, Trucks GW, Schlegel HB, Scuseria GE, Robb MA et al. (2013) Gaussian 09, revision D. 01. Gaussian, Inc, Wallingford
15. Blomberg MRA, Borowski T, Himo F, Liao RZ, Siegbahn PE (2014) Quantum chemical studies of mechanisms for metalloenzymes. Chem Rev 114:3601–3658
16. Shaik S, Cohen S, Wang Y, Chen H, Kumar D, Thiel W (2009) P450 enzymes: their structure, reactivity, and selectivity modeled by QM/MM calculations. Chem Rev 110:949–1017
17. Yano JK, Wester MR, Schoch GA, Griffin KJ, Stout CD, Johnson EF (2004) The structure of human microsomal cytochrome P450 3A4 determined by X-ray crystallography to 2.05-A resolution. J Biol Chem 279:38091–38094
18. Chen Z, Kang Y, Zhang C, Tao J, Xue Y (2015) Metabolic mechanisms of caffeine catalyzed by cytochrome P450 isoenzyme 1A2: a theoretical study. Theor Chem Accounts 134:1–14
19. Tao J, Kang Y, Xue ZY, Wang YT, Zhang Y, Chen Q, Chen ZQ, Xue Y (2015) Theoretical study on the N-demethylation mechanism of theobromine catalyzed by P450 isoenzyme 1A2. J Mol Graph Model 61:123–132
20. Kwiecień RA, Molinié R, Paneth P, Silvestre V, Lebreton J, Robins RJ (2011) Elucidation of the mechanism of N-demethylation catalyzed by cytochrome P450 monooxygenase is facilitated by exploiting nitrogen-15 heavy isotope effects. Arch Biochem Biophys 510:35–41
21. Li D, Wang Y, Yang C, Han K (2009) Theoretical study of N-dealkylation of N-cyclopropyl-N -methylaniline catalyzed by cytochrome P450: insight into the origin of the regioselectivity. Dalton Trans 2:291–297
22. Wang Y, Wang HM, Wang YH, Yang CL, Yang L, Han KL (2006) Theoretical study of the mechanism of acetaldehyde hydroxylation by compound I of CYP2E1. J Phys Chem B 110:6154–6159
23. Kang Y, Tao J, Xue ZY, Zhang Y, Chen ZQ, Xue Y (2016) Quantum chemical exploration on the metabolic mechanisms of caffeine by flavin-containing monooxygenase. Tetrahedron 72: 2858–2867
24. Xue ZY, Zhang Y, Tao J, Kang Y, Chen ZQ, Xue Y (2016) Theoretical elucidation of the metabolic mechanisms of phenothiazine neuroleptic chlorpromazine catalyzed by cytochrome P450 isoenzyme 1A2. Theor Chem Accounts 135:218. doi:10.1007/s00214-016-1943-4

25. Zhang Q, Bell R, Truong TN (1995) Ab initio and density functional theory studies of proton transfer reactions in multiple hydrogen bond systems. J Phys Chem 99:592–599
26. Reed AE, Schleyer PVR (1990) Chemical bonding in hypervalent molecules. The dominance of ionic bonding and negative hyperconjugation over d-orbital participation. J Am Chem Soc 112:1434–1445
27. Schröder D, Shaik S, Schwarz H (2000) Two-state reactivity as a new concept in organometallic chemistry. Acc Chem Res 33:139–145
28. Baciocchi E, Bietti M, Gerini MF, Lanzalunga O (2005) Electron-transfer mechanism in the N-demethylation of N, N-dimethylanilines by the phthalimide-N-oxyl radical. J Org Chem 70:5144–5149
29. Guengerich FP, Yun CH, Macdonald TL (1996) Evidence for a 1-electron oxidation mechanism in N-dealkylation of N, N-dialkylanilines by cytochrome p450 2b1 kinetic hydrogen isotope effects, linear free energy relationships, comparisons with horseradish peroxidase, and studies with oxygen surrogates. J Biol Chem 271:27321–27329
30. Jurva U, Bissel P, Isin EM, Igarashi K, Kuttab S, Castagnoli N (2005) Model electrochemical-mass spectrometric studies of the cytochrome P450-catalyzed oxidations of cyclic tertiary allylamines. J Am Chem Soc 127:12368–12377
31. Li C, Wu W, Kumar D, Shaik S (2006) Kinetic isotope effect is a sensitive probe of spin state reactivity in CH hydroxylation of N, N-dimethylaniline by cytochrome P450. J Am Chem Soc 128:394–395
32. Chen H, de Groot MJ, Vermeulen NP, Hanzlik RP (1997) Oxidative N-dealkylation of p-cyclopropyl-N, N-dimethylaniline. A substituent effect on a radical-clock reaction rationalized by ab initio calculations on radical cation intermediates. J Org Chem Rev 62:8227–8230